Discrete Electronic Bands in Semiconductors and Insulators: Potential High-Light-Yield Scintillators

Hongliang Shi and Mao-Hua Du

Phys. Rev. Applied **3**, 054005 — Published 12 May 2015

DOI: 10.1103/PhysRevApplied.3.054005

Discrete electronic bands in semiconductors and insulators: Potential high-light-yield scintillators

Hongliang Shi and Mao-Hua Du

Materials Science & Technology Division and Center for Radiation Detection Materials and Systems, Oak Ridge National Laboratory, Oak Ridge, TN 37831, USA

Bulk semiconductors and insulators typically have continuous valence and conduction bands. Here, we show that valence and conduction bands of a multinary semiconductor or insulator can be split to narrow discrete bands separated by large energy gaps. This unique electronic structure is demonstrated by first-principles calculations in several quaternary elpasolite compounds, i.e., $Cs_2NaInBr_6$, $Cs_2NaBiCl_6$, and $Tl_2NaBiCl_6$. The narrow discrete band structure in these quaternary elpasolites is due to the large electronegativity difference among cations and the large nearest-neighbor distances in cation sublattices. We further use $Cs_2NaInBr_6$ as an example to show that the narrow bands can stabilize self-trapped and dopant-bound excitons (in which both the electron and the hole are strongly localized in static positions on adjacent sites) and promote strong exciton emission at room temperature. The discrete band structure should further

suppress thermalization of hot carriers and may lead to enhanced impact ionization, which is usually considered inefficient in bulk semiconductors and insulators. These characteristics can enable efficient room-temperature light emission in low-gap scintillators and may overcome the light-yield bottleneck in current scintillator research.

PACS: 71.35.Aa, 71.38.Ht, 71.55.-i

I. Discrete electronic bands in semiconductors and insulators

A. Introduction

Bulk semiconductors and insulators typically have continuous valence and conduction bands as schematically shown in Figure 1(a). Discrete energy levels and bands have been sought after for various applications. For instance, discrete energy levels existing in semiconductor nanocrystals, or quantum dots (QDs) [see Figure 1(b)] have been proposed as a way to suppress hot carrier thermalization and to enhance carrier multiplication in QD solar cells.[1, 2, 3] Impurity bands in the band gap [see Figure 1(c)] have been introduced for intermediate-band solar cells[4, 5, 6, 7] and for efficient visible light absorption and photocatalysis.[8, 9, 10] In this paper, we show in Sec. I that narrow discrete energy bands, which result from the splitting of the conduction and valence bands, can form in bulk semiconductors [see Figure 1(d)]; in Sec. II, we further discuss why scintillator materials can benefit from such electronic structure, leading to improved light yield and energy resolution.

In a semiconductor, core electronic states have little dispersion in the band structure. On the other hand, the valence electrons of neighboring atoms have significant interaction; therefore, their states form wide energy bands. The width of the energy band should increase with hybridization strength between atomic orbitals, which depends on the spatial and energy separations between these orbitals.

In a multinary compound semiconductor, the electronic states of different cations (anions) mix to form conduction (valence) bands. The lower part of the conduction (valence) band is made up of the electronic states derived from more electronegative cations (anions) while the higher part of the conduction (valence) band is made up of

those from less electronegative cations (anions). In principle, the conduction or valence band can even be split (as schematically shown in Fig. 1(d)) if there is a large electronegativity difference between different types of cations or anions. Also, in a compound with multiple types of cations (anions), the nearest-neighbor distance in a cation (anion) sublattice can be much longer than that in a binary compound. This should lead to narrower electronic bands, further increasing the energy gaps between the separated conduction or valence bands. Therefore, we suggest that a combination of large electronegativity difference between different cations (anions) and large nearest-neighbor distances in cation (anion) sublattices in a multinary compound may lead to the splitting of the conduction (valence) band, resulting in several narrow discrete electronic bands separated by large energy gaps. This can be used as a materials selection guide for finding narrow discrete energy bands in bulk semiconductors.

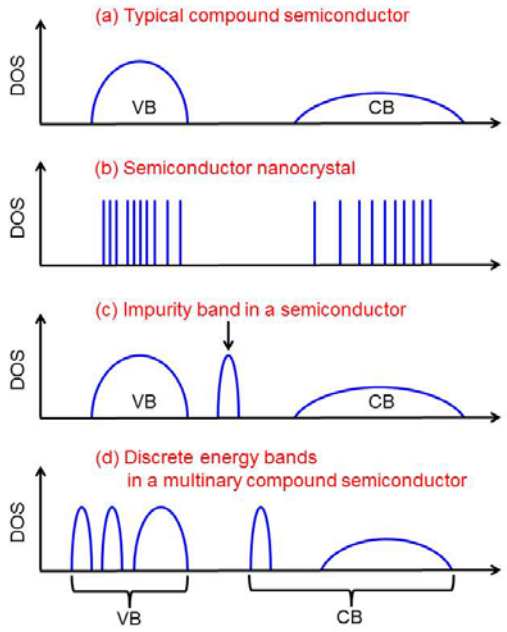

FIGURE 1. Schematic figures of density of states for (a) a typical bulk compound semiconductor; (b) a semiconductor nanocrystal; (c) an impurity band in a semiconductor; and (d) discrete energy bands in a multinary compound semiconductor.

The narrow discrete band structure can be realized in elpasolites, which have properties consistent with the above materials selection guide. Elpasolites are a large family of quaternary halides, $A_2BB'X_6$, where A and B are monovalent cations, B' is an trivalent cation, and X is a halogen anion (see Fig. 2).[11] Many elpasolites have cubic double-perovskite structure. BX_6 and $B'X_6$ form corner-shared octahedral network, in which B and B' are ordered in rocksalt symmetry. Previous studies on Cs_2LiYCl_6 and Cs_2AgYCl_6 elpasolites[12, 13] show that the conduction band of an elpasolite compound can be split. Taking Cs_2LiYCl_6 as an example, the electronegativity of Y (1.22) is much higher than those of Cs (0.79) and Li (0.98) and the nearest-neighbor Y-Y distance is long at 7.4 Å. Consequently, the Y-3d states form a narrow conduction band, split slightly from the higher-energy Cs and Li bands.[12] In this paper, we show that chemical substitutions can be used to manipulate the electronegativities of the constituent elements in elpasolites and demonstrate cases that allow further control and tuning of the energy splitting of both conduction and valence bands, leading to much smaller band gaps and much larger energy splitting than those in Cs_2LiYCl_6.

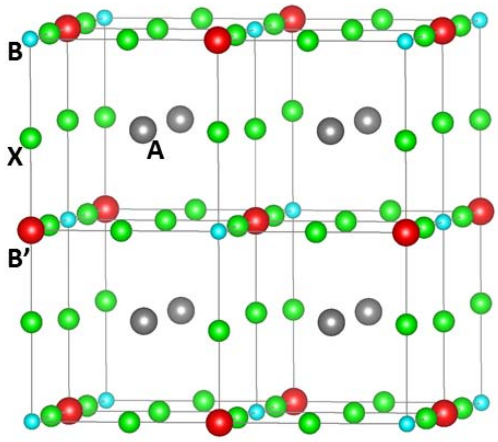

Figure 2. Structure of an elpasolite ($A_2BB'X_6$) compound.

B. Results: Electronic structure of $Cs_2NaInBr_6$, $Cs_2NaBiCl_6$, and $Tl_2NaBiCl_6$

Figure 3 shows the band structure and density of states (DOS) of $Cs_2NaInBr_6$, calculated using hybrid functionals (PBE0),[14] which have a 25% Hartree-Fock exchange, within density functional theory (DFT).[15] The PBE0 band gap of Cs_2LiYCl_6 has previously been shown to be in good agreement with the experimental value.[12] $Cs_2NaInBr_6$ has a cubic structure with a lattice constant of 11.103 Å[16] and a direct band gap at the Γ point as shown in Fig. 3(a). The PBE0 band gap of $Cs_2NaInBr_6$ is 3.84 eV.

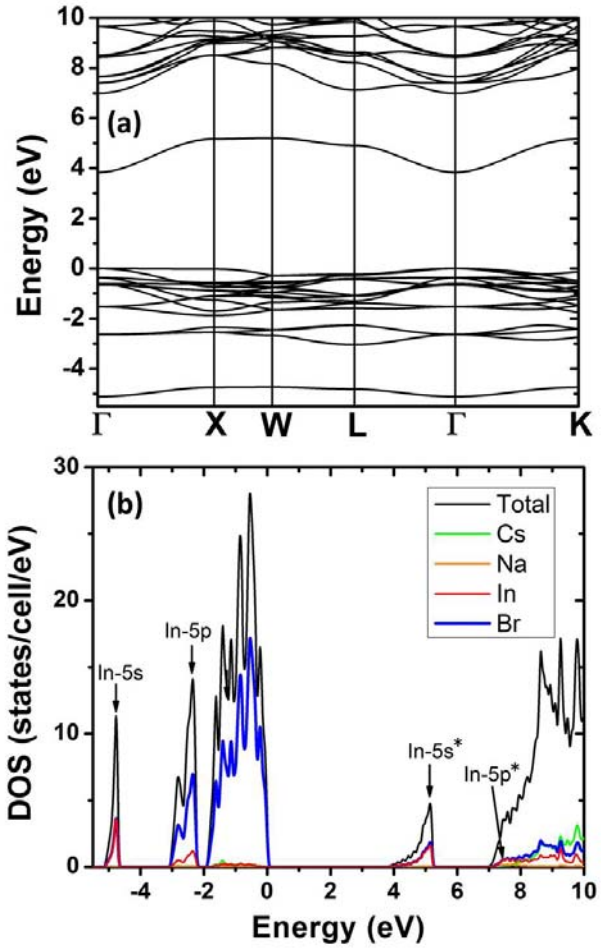

FIGURE 3. (a) Band structure and (b) projected density of states (DOS) of $Cs_2NaInBr_6$ calculated using PBE0 functionals. The main In-related bands are labeled in (b) according to the orbital character of In states (5s or 5p) and the bonding character [bonding or antibonding (antibonding states are labeled with an asterisk)]. See text for details.

The DOS of $Cs_2NaInBr_6$ shows that the conduction and valence bands are both split due to the large electronegativity difference between In (1.78) and Cs/Na (0.79/0.93). The conduction band is split with a giant energy gap. The lower conduction band is a narrow band of only 1.4 eV in width. It is made up of In-5s states hybridized with Br-4p states. The higher conduction band is a wider band with In-5p and Cs/Na states. The In-5s derived conduction band is separated from the Br-4p-derived valence band and the In-5p and Cs/Na dominated higher conduction band by large energy gaps, appearing almost like an isolated impurity band. The narrowness of the In-5s-derived conduction band should be due to the long In-In nearest-neighbor distance (7.85 Å) and the resulting weak In-In hybridization. The valence band of $Cs_2NaInBr_6$ is also split. The narrow bands around -5 eV and -3 eV in Fig. 3(b) are mainly made up of Br-4p states hybridized with In-5s and In-5p states, respectively. The higher valence band is only about 2 eV in width.

Figure 4 shows the band structure and DOS of $Cs_2NaBiCl_6$, another example of discrete bands in elpasolites. Bi has a high electronegativity of 2.02. $Cs_2NaBiCl_6$ has a cubic structure, a lattice constant of 10.839 Å,[17] and an indirect band gap of 4.64 eV calculated using PBE0 functionals. The valence band maximum (VBM) and the conduction band minimum (CBM) are located at the W point and the Γ point, respectively. The conduction band is split to lower Bi-6p derived bands and higher Cs/Na dominated bands. The Bi-6p bands are further split by the strong spin-orbit coupling, giving rise to two Bi-6p peaks in DOS (see Fig. 4(b)). The lower Bi-6p band is an extremely narrow band with a band width of only 0.36 eV. Similar to the conduction band, the valence band is also split. The two Bi-6p-related narrow bands (hybridized with

Cl 3p states) are located around -3 eV and -3.5 eV respectively (Fig. 4). The top of the valence band has a strong Bi-6s character due to the hybridization between the occupied Bi-6s states (about 9 eV below the VBM) and the Cl 3p states.

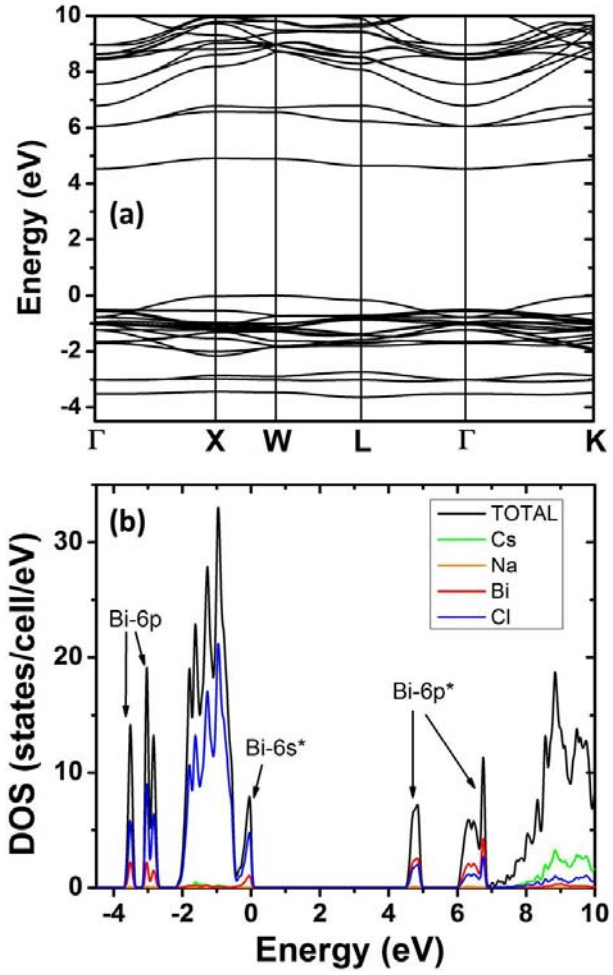

FIGURE 4. (a) Band structure and (b) projected density of states (DOS) of $Cs_2NaBiCl_6$ calculated using PBE0 functionals. The main Bi-related bands are labeled in (b) according to the orbital character of Bi states (6s or 6p) and the bonding character [bonding or antibonding (antibonding states are labeled with an asterisk)]. See text for details. The antibonding Bi-6s* states are shown to be near the VBM while the bonding Bi-6s states form a narrow band nearly 9 eV below the VBM (not shown). Spin-orbit coupling is included in the calculations.

One can also manipulate the electronegativity of the A site ion in elpasolites ($A_2BB'X_6$) as shown in Fig. 5 for $Tl_2NaBiCl_6$, which has a pseudocubic structure and a

lattice constant of 10.60 Å.[18] Here, the conduction band is split due to the energy separation of the 6p states of Tl and Bi from the Na states. The Tl and Bi 6p bands are further split by spin-orbit coupling. The valence band is also split with Tl and Bi 6p related bands (hybridized with the Cl 3p states) located between -3 eV and -5 eV in Fig. 5(b).

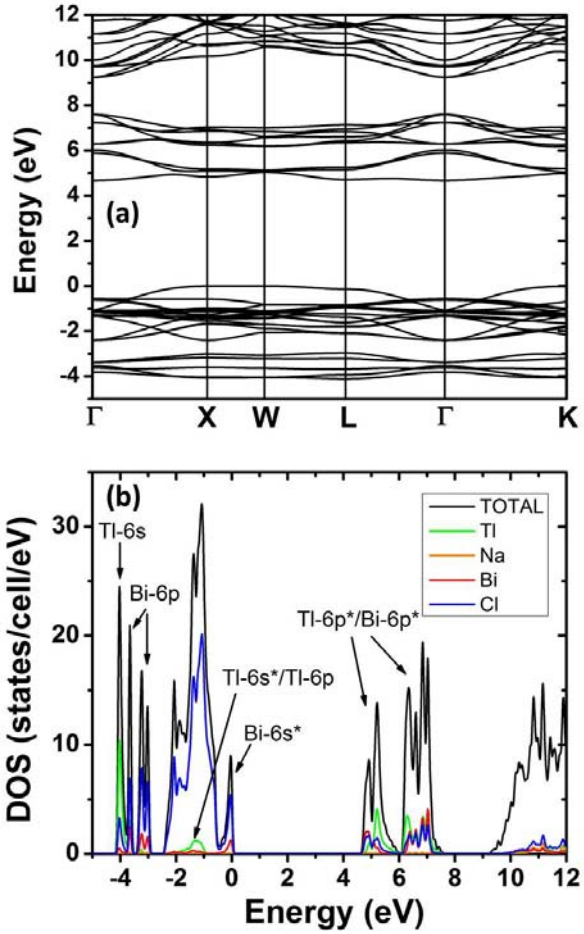

FIGURE 5. (a) Band structure and (b) projected density of states (DOS) of $Tl_2NaBiCl_6$ calculated using PBE0 functionals. The main Tl- and Bi-related bands are labeled in (b) according to the orbital character of Tl and Bi states (6s or 6p) and the bonding character [bonding or antibonding (antibonding states are labeled with an asterisk)]. See text for details. The antibonding Bi-6s* states are shown to be near the VBM while the bonding Bi-6s states form a narrow band nearly 9 eV below the VBM (not shown). The Tl-6s* antibonding states and the Tl-6p bonding states are resonant in the valence band, around 1 – 2 eV below the VBM. Spin-orbit coupling is included in the calculations.

The electronic structure calculations for $Cs_2NaInBr_6$, $Cs_2NaBiCl_6$, and $Tl_2NaBiCl_6$ demonstrate that the narrow discrete energy bands can be realized in bulk multinary compounds. Next we show how such unique electronic structure can be extremely useful for a scintillator.

II. Low-band-gap scintillators with discrete electronic bands

A. Introduction

A scintillator can emit photons upon exposure to high-energy x-rays or gamma-rays and therefore is widely used for radiation detection.[19] The light yield is one of the most important measures of scintillator performance. A higher light yield can potentially lead to better energy resolution of a scintillator.[19] The light yield, which is typically measured in terms of the number of photons per MeV of radiation energy, is given by

$$L = \frac{SQ}{\beta E_g} \times 10^6 \text{ photons/MeV}, \quad (1)$$

where E_g is the band gap expressed in eV, Q is the quantum efficiency of the activator, S is the energy transfer efficiency to luminescent centers or activators, which are typically found in scintillators. Some scintillators are self-activated. For example, electrons and holes can form excitons bound to native atoms (such as Ce^{3+} in $CeBr_3$) or induce structural distortion to form self-trapped excitons (STEs) followed by radiative recombination. In these cases, S in Eq. 1 can be redefined to be the probability of an electron and a hole to form a bound exciton or a STE and Q is the quantum efficiency of an exciton. βE_g is the energy needed to create an electron-hole pair. β reflects the fact that only a fraction of the radiation energy is used to excite electron-hole pairs. The rest is lost

to phonons. β is typically higher in covalent materials (3 to 4) than in ionic materials (1.5 to 2.0) due to the more efficient energy transfer to phonons in covalent materials.[19]

For several high-light-yield scintillators, such as SrI_2, their light yields are already close to their theoretical limits. For example, a light yield of 120000 photons/MeV has been reported for SrI_2.[20] If one takes the ideal conditions, i.e., $SQ = 1$ and $\beta = 1.5$ in Eq. 1, and uses the 5.2-eV band gap calculated using the GW method,[21] one gets ~128000 photons/MeV, only slightly higher than the highest reported light yield of SrI_2. Therefore, to further increase the light yield, one has to look for materials with smaller band gaps.

Scintillators are usually insulators with large band gaps. The use of lower-gap materials as scintillators have several challenges, e.g., (1) the band gap is too small to accommodate activator levels, which are needed to trap both electrons and holes;[22] (2) β in Eq. 1 tends to increase with decreasing band gap.[19] These two problems have largely prevented the practical use of many semiconductors as scintillators. For example, ZnO and PbI_2 (which have small band gaps of 3.4 eV and 2.5 eV,[23] respectively) are fast scintillators but suffer from thermal quenching and low light yield at room temperature.[24] The leading scintillator materials, such as NaI:Tl^+, $LaBr_3$:Ce^{3+}, and SrI_2:Eu^{2+}, all have band gaps larger than 5 eV. In this paper, we show that the narrow discrete energy bands of some low-gap elpasolites can resolve the above two problems and potentially lead to higher light yield.

For efficient luminescence at room temperature, activators are often used in inorganic scintillators and phosphors to trap electrons and holes deep enough to avoid thermal quenching. Some activators insert two levels in the host band gap, e.g., 4f and 5d levels of rare-earth ions (e.g., Ce^{3+} and Eu^{2+})[12, 25, 26, 27] and np and ns levels of ns^2 ions

(e.g., Tl^+)[28, 29, 30, 31], each of which traps one type of carrier, either an electron or a hole. Some other activators insert one level that traps one type of carrier while relying on the self-trapping of the other type of carrier. For example, Tl^+ in CsI traps electrons on its 6p level while the hole self-traps as a V_k center, which migrates to bind with Tl^0 to form a Tl-bound exciton before radiative recombination.[31] As the band gap shrinks, it becomes increasingly difficult for the above two type of activators to facilitate radiative recombination of carriers, because (1) a small band gap is difficult to accommodate two activator levels; and (2) a low-gap material is usually more covalent and thus makes carrier self-trapping energetically unfavorable.

Many elpasolites ($A_2^+B^+B'^{3+}X_6^-$) can be activated by Ce^{3+}, which is isovalent to the B'^{3+} ion. We have previously studied Ce^{3+} activated elpasolites with the goal of finding elpasolites whose band gaps are small enough to allow high light yield but still large enough to accommodate the Ce 4f and 5d levels.[12,13] However, the need to accommodate both Ce 4f and 5d levels in the band gap limits how small the band gap can be and consequently caps the light yield.

Excitons in semiconductors can emit photons. However, the exciton binding energies are usually too small to stabilize excitons at room temperature. In halides, the small hole polaron, or V_k center, is usually quite stable due to the small valence band dispersion. However, the conduction band in many halides, such as alkali halides, is much more dispersive.[31] Therefore, the delocalized electron is only loosely bound to the localized small hole polaron in alkali halides, forming a STE, whose emission is observed at low temperatures but quenched at room temperature.[32] The light yields of undoped NaI and CsI are very high at liquid nitrogen temperature (>80000 phtons/MeV for NaI and

>100000 phtons/MeV for CsI) but are quenched at room temperature.[33, 34, 35] Elpasolites have much narrower conduction bands[12,13] than alkali halides, leading to enhanced electron localization near a small hole polaron and hence more stable STEs. Below we use $Cs_2NaInBr_6$ as an example to show that scintillation in low-gap elpasolites is possible without Ce doping.

B. Computational methods

The binding energies of polarons and self-trapped and dopant-bound excitons in $Cs_2NaInBr_6$ were calculated using PBE0 functionals following Ref. 12. A charge transition level $\varepsilon(q/q')$ of a self-trapped carrier or exciton is given by

$$\varepsilon(q/q') = \frac{E_{D,q'} - E_{D,q}}{q - q'}, \tag{2}$$

where $E_{D,q}$ ($E_{D,q'}$) is the total energy of the supercell that contains the relaxed structure of a defect at charge state q (q').

The binding energies of hole and electron polarons (or the energies of hole and electron polarons relative to those of a free hole and a free electron) are $\Delta B_{hole-pol} = \varepsilon_{hole-pol}(+/0) - \varepsilon_v = E_0 - E_{hole-pol} - \varepsilon_v$ and $\Delta B_{el-pol} = \varepsilon_c - \varepsilon_{el-pol}(0/-) = \varepsilon_c - E_{el-pol} + E_0$, respectively. Here, ε_V and ε_c are the energies of the VBM and CBM, respectively. $\varepsilon_{hole-pol}(+/0)$ and $\varepsilon_{el-pol}(0/-)$ are the transition levels for the hole and the electron polarons, respectively. E_0 is the energy of the neutral defect-free supercell and $E_{hole-pol}$ and E_{el-pol} are the energies of the supercells

that contain relaxed hole and electron polarons, respectively. Here, a positive binding energy corresponds to stable binding.

The binding energy of a STE relative to an electron and a hole polarons is given by $\Delta B_{\mathrm{STE}} = E_{\mathrm{STE}} + E_0 - E_{hole-pol} - E_{el-pol}$, where E_{STE} is the energy of the supercell that contains a relaxed STE. The relaxed STE structure was obtained by adding an electron to the supercell that contains a small hole polaron followed by structural optimization in a triplet spin configuration (a triplet STE). The electron and the hole in the STE studied in this work are both trapped by deep levels in the band gap and are spatially highly localized. There are significant structural distortions associated with the hole and electron localization. The calculated total energy of a relaxed STE includes the Coulomb interaction between the electron and the hole and the structural relaxation energy. The sum of ΔB_{STE}, $\Delta B_{hole-pol}$, and ΔB_{el-pol} gives the binding energy of a STE relative to a free electron and a free hole.

If the $\varepsilon_{el-pol}(0/-) > \varepsilon_c$ ($\Delta B_{el-pol} < 0$), the electron polaron is metastable (less stable than a free electron). In this case, the stability of a STE is determined by the binding energy between a hole polaron and a free electron, which is given by either $\Delta B_{\mathrm{STE}} + \Delta B_{el-pol}$ or $\varepsilon_c - \varepsilon(+/0^*)$. [$\varepsilon(+/0^*)$ is the charge transition level between a hole polaron and a neutral STE.] The two approaches are equivalent and give the identical results.

The energies of trapping a hole at a dopant and the subsequent trapping of an electron at the dopant-induced localized hole center can be calculated in similar ways as described above for a STE.

A 40-atom cubic supercell and 2×2×2 k-mesh for Brillouin zone integration were used for the above calculations. Image charge and potential alignment corrections were performed wherever appropriate.[36] Due to the narrow conduction and valence bands and the resulting strong charge localization, the binding energies of polarons and self-trapped and dopant-bound excitons can be calculated using a relatively small 40-atom supercell with reasonable accuracy. Previous calculations on Cs_2LiYCl_6 showed that the hole polaron binding energy is increased by 0.07 eV by increasing the supercell size to contain 80 atoms.[12] Using larger cells allows better structural relaxation of structurally distorted self-trapped carriers and excitons and thus should lead to larger binding energies.

C. Results: Polarons and self-trapped and iodine-bound excitons in $Cs_2NaInBr_6$

$Cs_2NaInBr_6$ has a relatively small band gap. The PBE0 band gap of $Cs_2NaInBr_6$ is 3.84 eV, much smaller than those of rare-earth elpasolites, e.g., the calculated band gaps of Cs_2LiYCl_6, $Cs_2NaLaBr_6$, and Cs_2NaYBr_6 are 7.08 eV, 6.31 eV, and 6.25 eV, respectively.[12, 37] The smaller band gap of $Cs_2NaInBr_6$ compared to those of rare-earth elpasolites is largely due to the much more electronegative In and consequently lower conduction band. Our calculations show that the low CBM in $Cs_2NaInBr_6$ cannot accommodate the Ce 5d levels within the band gap; therefore, $Cs_2NaInBr_6$ cannot be activated by Ce^{3+}. However, the very narrow conduction and valence bands of $Cs_2NaInBr_6$ (as shown in Fig. 3) may stabilize STEs even at room temperature because narrow bands enhance charge localization.[38]

A free hole in $Cs_2NaInBr_6$ self-traps to form a small hole polaron by moving two Br ions close to each other (the calculated Br-Br distance is 2.85 Å), as shown in Fig.

6(a). This is a typical V_k center found in many halides. The small hole polaron binding energy is calculated to be 0.36 eV (see Fig. 7), which is large enough to make a hole polaron stable at room temperature. We also found that an electron can be localized around an In ion, forming a small electron polaron. The electron self-trapping or self-localization at an In ion increases the six surrounding In-Br bond lengths from 2.67 Å to 2.81 Å. The single-particle level that traps the electron is a deep level at E_c – 0.87 eV. The calculated (0/-) thermodynamic transition level for an electron polaron is 0.2 eV above the CBM, indicating that the electron polaron is metastable.

Although a self-localized electron is less stable than a free electron by 0.2 eV, strong electron localization is energetically favored near a small hole polaron. Our calculations show that a small hole polaron can trap an electron with a substantial binding energy of 0.3 eV (Fig. 7), resulting in a STE that is stable at room temperature. The total binding energy of a STE relative to a free electron and a free hole is calculated to be 0.67 eV. In a STE, the electron and the hole are trapped by two deep single-particle levels, i.e., E_c – 1.09 eV and E_v + 2.28 eV, respectively, inside the band gap. The single-particle level that traps the electron (E_c – 1.09 eV) is derived from the In-5s orbitals and is localized at the In ion adjacent to the small hole polaron. The charge density contours of the electron and the hole states in the STE are shown in Fig. 6. It can be seen that both the electron and the hole are highly localized in the STE, consistent with their deep single-particle levels. The deep electron trapping in the STE is accompanied by the local structural distortion, i.e., the In-Br1 and In-Br2 bond lengths in Fig. 6 increases from 2.81 Å (in a small hole polaron) to 2.99 Å (in a STE) upon the electron trapping.

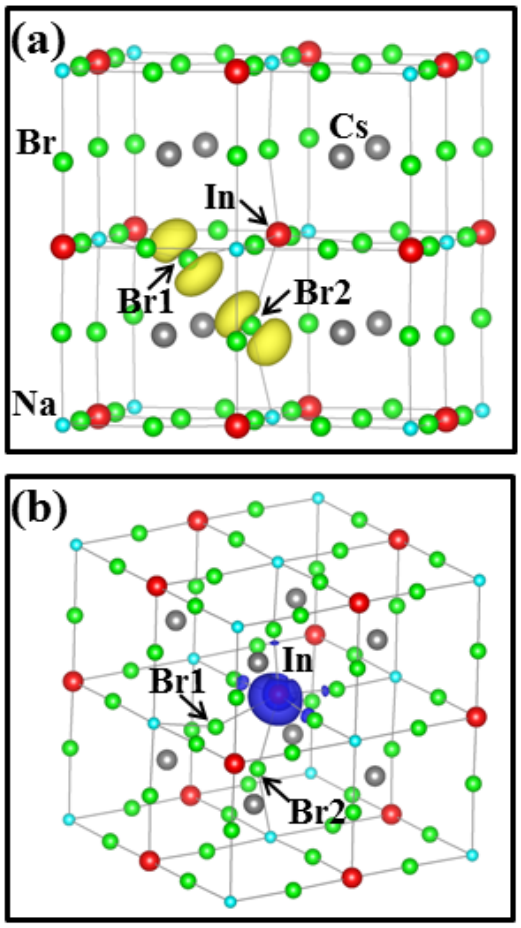

Figure 6. Isosurfaces of partial charge densities of (a) the localized hole state and (b) the localized electron state in a STE. In the STE, the hole is localized at the Br1 and Br2 ions and the electron is localized at the In ion adjacent to both Br1 and Br2 ions. The charge densities of the isosurfaces in (a) and (b) are 0.006 and -0.006 e/bohr^3, respectively.

The STE emission energy is calculated to be 1.39 eV, which is the total energy difference between the STE and the ground state both at the STE structure. The large calculated STE binding energy suggests that STE emission in $Cs_2NaInBr_6$ should be strong even at room temperature. The room temperature STE emission in both undoped and Ce doped Cs_2LiYCl_6 has indeed been reported.[39, 40] Note that the calculated band gap of $Cs_2NaInBr_6$ (3.84 eV) is much smaller than that of Cs_2LiYCl_6 (7.08 eV). The large

STE binding energy in such a low-gap material as $Cs_2NaInBr_6$ is caused by the narrow discrete conduction band that promotes the electron localization.

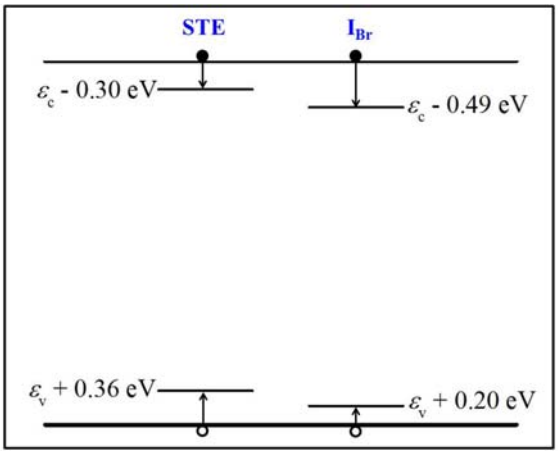

FIGURE 7. The hole and electron trapping levels at a STE and at an I_{Br} in $Cs_2NaInBr_6$: the hole self-trapping level ($\varepsilon(+/0)=\varepsilon_v$ + 0.36 eV) and the hole trapping level at I_{Br} ($\varepsilon(+/0)=\varepsilon_v$ + 0.20 eV); the electron trapping level at a small hole polaron ($\varepsilon(+/0^*)=\varepsilon_c$ - 0.30 eV) and at an I_{Br}^+ ($\varepsilon(+/0^*)=\varepsilon_c$ - 0.49 eV).

Since a free electron can be strongly bound to a small hole polaron, it should also be bound to other localized hole centers. One can introduce a dopant to facilitate the formation of an acceptor-like bound exciton. For example, iodine can be doped into $Cs_2NaInBr_6$ to trap holes. The PBE0 calculations show that I on a Br site (I_{Br}) introduces a fully occupied single-particle level of 0.22 eV above the VBM. The I level is isolated from the Br dominated valence band because of the narrowness of the valence band. A hole can be trapped at the I level with a binding energy of 0.20 eV (Fig. 7). A free electron can further bind with I_{Br}^+ and become localized with a binding energy of 0.49 eV (Fig. 7). The trapping of a free hole and a free electron at I_{Br} forms an I_{Br}-bound exciton and lowers the total energy by 0.69 eV. The structural distortion at an I_{Br}-bound exciton is significantly less than that at a STE (which involves large displacement of two Br ions to form a charged Br_2^- molecule), leading to a larger exciton emission energy, which is

calculated to be 2.53 eV (490 nm). This is compared to 1.39 eV (893 nm) calculated for a STE. The 490 nm emission wavelength is close to that of CsI:Tl (530 nm).[41] The emission band width of the I_{Br}-bound excitons is expected to be narrower than that of the STEs due to less phonon involvement. The scintillation decay time for I_{Br}-bound excitons may be shorter than that for STEs since the stronger spin-orbit coupling due to the heavy iodine ions mixes the spin-triplet and -singlet states and thus promotes fast light emission.

D. Discussion

The stability of self-trapped and dopant-bound excitons and the emission wavelength can be tuned by alloying (e.g., $Cs_2NaInBr_{6-x}Cl_x$). For example, increasing the Cl concentration in $Cs_2NaInBr_{6-x}Cl_x$ should increase the ionicity of the material and enhance charge localization, leading to more stable excitons. Also, the band gap should increase with the Cl concentration, thereby, shortening the exciton emission wavelength and reducing the number of excitons created by radiation. Thus, alloying may be used for reducing thermal quenching of exciton emission and for tuning the exciton emission wavelength to better couple with the sensitivity of the photodetector. However, light yield may be reduced if the band gap is increased by alloying.

The narrow discrete conduction and valence bands not only promote exciton-based luminescence at room temperature, but also create phonon bottlenecks (electronic energy gaps much larger than phonon energies), which prevent efficient transfer of energy from hot carriers to phonons.[42, 43, 44] If hot carrier thermalization is slowed, other competing processes, such as impact ionization (which is usually considered inefficient in bulk semiconductors due to fast carrier thermalization in continuous energy bands), may

take place more efficiently. Taking $Cs_2NaInBr_6$ as an example, a hole in the narrow band that is more than 4 eV below the VBM [see Fig. 3(a)] can relax to the VBM. The released energy can be transferred to an electron in the valence band, promoting it to the conduction band (which requires energy more than the band gap energy of 3.84 eV). The energy and momentum conservation can be satisfied in this process. The reduced hot carrier thermalization and the enhanced impact ionization should lower β in Eq. 1, leading to higher light yield.

In $Cs_2NaInBr_6$, the lower conduction band is derived from In-5s states and the higher conduction band has a significant In-5p component (see Fig. 3(b)). This may lead to In 5p→5s emission (inter-conduction-band luminescence). Such hot carrier luminescence can also contribute to the total light yield.

III. Conclusions

First-principles calculations show that the conduction and valence bands of a multinary semiconductor/insulator can be split to narrow discrete bands by a combination of large electronegativity difference among cations or anions and large nearest-neighbor distances in cation or anion sublattices. This concept is demonstrated by first principles calculations of several quaternary elpasolite compounds, i.e., $Cs_2NaInBr_6$, $Cs_2NaBiCl_6$, and $Tl_2NaBiCl_6$. Based on calculated polaron and exciton binding energies for $Cs_2NaInBr_6$, we find that the narrow conduction and valence bands promote the self-trapping of electrons and holes, which enhances the stabilization of self-trapped and dopant-bound excitons at room temperature. Both the electron and the hole in a STE or a iodine-bound exciton in $Cs_2NaInBr_6$ are found to be strongly localized on adjacent sites.

The exceptional stability of excitons provides an approach to activate exciton-based room-temperature light emission for low-gap scintillator materials. Furthermore, discrete bands with large energy separations (large phonon bottlenecks) in a scintillator should further suppress the hot carrier thermalization and may lead to more efficient impact ionization and higher light yield. A higher light yield can potentially improve the energy resolution of a scintillator. Finally, it should be pointed out that the narrow discrete band structures are not restricted to elpasolite compounds and should exist in many other multinary compound semiconductors and insulators.

Acknowledgements

The authors are grateful for the helpful discussion with David J. Singh, Hua Wei, Chuck L. Melcher, and Zane W. Bell. This work was supported by the Department of Energy, Office of Science, Basic Energy Sciences, Materials Sciences and Engineering Division.

---

[1] A. J. Nozik, Spectroscopy and hot electron relaxation dynamics in semiconductor quantum wells and quantum dots, Annu. Rev. Phys. Chem. **52**, 193 (2001).

[2] R. D. Schaller, V. I. Klimov, High efficiency carrier multiplication in PbSe nanocrystals: Implications for solar energy conversion, Phys. Rev. Lett. **92**, 186601 (2004).

[3] R. J. Ellingson, M. C. Beard, J. C. Johnson, P. Yu, O. I. Micic, A. J. Nozik, A. Shabaev, and A. L. Efros, Highly efficient multiple exciton generation in colloidal PbSe and PbS quantum dots, Nano Lett. **5**, 865 (2005).

[4] W. Wang, A. S. Lin, and J. D. Phillips, Intermediate-band photovoltaic solar cell based on ZnTe:O, Appl. Phys. Lett. **95**, 011103 (2009).

[5] N. Lopez, L. A. Reichertz, K. M. Yu, L. Campman, and W. Walukiewic, Engineering the electronic band structure for multiband solar cells, Phys. Rev. Lett. **106**, 028701 (2011).

[6] A. Luque, and A. Marti, Photovoltaics: Towards the intermediate band, Nature Photon. **5**, 137 (2011).

[7] A. Luque, A. Marti, and C. Stanley, Understanding intermediate-band solar cells, Nature Photon. **6**, 146 (2012).

[8] R. Asahi, T. Morikawa, T. Ohwaki, K. Aoki, and Y. Taga, Visible-Light photocatalysis in Nitrogen-Doped Titanium Oxides, Science **293**, 269 (2001).

[9] S. U. M. Khan, M. Al-Shahry, and W. B. Ingler, Efficient photochemical water splitting by a chemically modified n-TiO_2, Science **297**, 2243 (2002).

[10] W Zhu, X. Qiu, V. Iancu, X. Q. Chen, H. Pan, W. Wang, N. M. Dimitrijevic, T. Rajh, H. M. Meyer III, M. P. Paranthaman, G. M. Stocks, H. H. Weitering, B. Gu, G. Eres, and Z. Zhang, Band gap narrowing of Titanium Oxide semiconductors by noncompensated Anion-Cation codoping for enhanced Visible-Light photoactivity, Phys. Rev. Lett. **103**, 226401 (2009).

[11] G. Meyer, The synthesis and structures of complex rare-earth halides, Prog. Solid State Chem. **14**, 141 (1982).

[12] K. Biswas and M. H. Du, Energy transport and scintillation of cerium-doped elpasolite Cs_2LiYCl_6: Hybrid density functional calculations, Phys. Rev. B **86**, 014102 (2012).

[13] M. H. Du and K. Biswas, Electronic structure engineering of elpasolites: Case of Cs_2AgYCl_6, J. Lumin. **143**, 710 (2013).

[14] J. P. Perdew, M. Ernzerhof, and K. Burke, Rationale for mixing exact exchange with density functional approximations, J. Chem. Phys. **105**, 9982 (1996).

[15] G. Kresse and J. Furthmüller, Efficient iterative schemes for ab initio total-energy calculations using a plane-wave basis set, Phys. Rev. B **54**, 11169 (1996).

[16] G. Meyer and H. Gaebell, Halo-Elpasolites, IV [1] on Bromo-Elpasolites $Cs_2B^IM^{III}Br_6$ (B^I = Li, Na; M^{III} = Sc, Y, La-Lu, In, V, Cr), Z. Naturforsch **33b**, 1476 (1978).

[17] L. R. Morss and W. R. Robinson, Crystal structure of $Cs_2NaBiCl_6$, Acta Cryst. **B28**, 653 (1972).

[18] B. V. Beznosikov and S. V. Misyul, The crystal chemistry of halide compounds of type $A_2B^+B^{3+}X_6$, Kristallografiya **23**, 346 (1978).

[19] Piotr A. Rodnyi, "Physical processes in inorganic scintillators", CRC Press, Boca Raton (1997).

[20] E. V. van Loef, C. M. Wilson, N. J. Cherepy, G. Hull, S. A. Payne, W. –S. Choong, W. W. Moses, and K. S. Shah, Crystal growth and scintillation properties of Strontium Iodide scintillators, IEEE Trans. Nucl. Sci. **56**, 869 (2009).

[21] P. Erhart, A. Schleife, B. Sadigh, and D. Åberg, Quasiparticle spectra, absorption spectra, and excitonic properties of NaI and SrI_2 from many-body perturbation theory, Phys. Rev. B **89**, 075132 (2014).

[22] A. Bessiere, P. Dorenbos, C. W. E. van Eijk, K. W. Kramer, H. U. Gudel, C. D. Donega, and A. Meijerink, Luminescence and scintillation properties of the small band gap compound $LaI_3:Ce^{3+}$, Nucl. Instrum. Meth. Phys. Res. A, **537**, 22 (2005).

[23] Springer Materials, http://www.springermaterials.com/docs/index.html.

[24] W. W. Moses, Current trends in scintillator detectors and materials, Nucl. Instrum. Meth. Phys. Res. A **487**, 123 (2002).

[25] P. Dorenbos, Scintillation mechanisms in Ce^{3+} doped halide scintillators, phys. stat. sol. (a) **202**, 195 (2005).

[26] M. D. Birowosuto and P. Dorenbos, Novel γ- and X-ray scintillator research: on the emission wavelength, light yield and time response of Ce^{3+} doped halide scintillators, phys. stat. sol. (a) **206**, 9 (2009).

[27] A. Canning, A. Chaudhry, R. Boutchko, and N. Grønbech-Jensen, First-principles study of luminescence in Ce-doped inorganic scintillators, Phys. Rev. B **83**, 125115 (2011).

[28] P. W. M. Jacobs, Alkali halide crystals containing impurity ions with the ns^2 ground-state electronic configuration, J. Phys. Chem. Sol. **52**, 35 (1991).

[29] A. Ranfagni, D. Mugnai, M. Bacci, G. Viliani, and M. P. Fontana, The optical properties of thallium-like impurities in alkali-halide crystals, Adv. Phys. **32**, 823 (1983).

[30] W. Beall Fowler, "Physics of color centers", edited by W. Beall Fowler, Academic Press Inc., New York (1968).

[31] M. H. Du, Chemical trends of electronic and optical properties of ns^2 ions in halides, J. Mater. Chem. C **2**, 4784 (2014).

[32] K. S. Song and R. T. Williams, "Self-Trapped Excitons", Springer-Verlag Berlin Heidelberg (1996).

[33] M. Moszyński, M. Balcerzyk, W. Czarnacki, M. Kapusta, W. Klamra, P. Schotanus, A. Syntfeld, and M. Szawlowski, Study of pure NaI at room and liquid Nitrogen temperatures, IEEE Trans. Nucl. Sci. **50**, 767 (2003).

[34] M. Moszyński, M. Balcerzyk, W. Czarnacki, M. Kapusta, W. Klamra, P. Schotanus, A. Syntfeld, M. Szawlowski, and V. Kozlov, Energy resolution and non-proportionality of the light yield of pure CsI at liquid nitrogen temperatures, Nucl. Instrum. Meth. Phys. Res. A **537**, 357 (2005).

[35] P. Schotanus, R. Kamermans, and P. Dorenbos, Scintillation characteristics of pure and T1-doped CsI crystals, IEEE Trans. Nucl. Sci. **37**, 177 (1990).

[36] S. Lany and A. Zunger, Assessment of correction methods for the band-gap problem and for finite-size effects in supercell defect calculations: Case studies for ZnO and GaAs, Phys. Rev. B **78**, 235104 (2008).

[37] H. Wei, H. Shi, M. H. Du, L. Stand, M. Zhuravleva, and C. L. Melcher, unpublished.

[38] Y. Toyozawa, "Electrons, holes, and excitons in deformable lattice", in *Relaxation of Elementary Excitations*, Springer Series in Solid State Sci. Vol. 18, pp 3-18, Ed. By R. Kubo and E. Hanamura (Springer, Berlin, Heidelberg, 1980).

[39] C. M. Combes, P. Dorenbos, C. W. E. van Eijk, K. W. Krämer, and H. U. Güdel, Optical and scintillation properties of pure and Ce^{3+}-doped Cs_2LiYCl_6 and $Li_3YCl_6 : Ce^{3+}$ crystals, J. Lumin. **82**, 299 (1999).

[40] A. Bessière, P. Dorenbos, C. W. E. van Eijk, L. Pidol, K. W. Krämer, and H. U. Güdel, Spectroscopy and anomalous emission of Ce doped elpasolite Cs_2LiYCl_6, J. Phys.: Condens. Matter **16**, 1887 (2004).

[41] B. C. Grabmaier, Crystal Scintillators, IEEE Transactions on Nuclear Science **31**, 372 (1984).

[42] U. Bockelmann and G. Bastard, Phonon scattering and energy relaxation in two-, one-, and zero-dimensional electron gases, Phys. Rev. B **42**, 8947 (1990).

[43] H. Benisty, C. M. Sotomayor-Terrès, and C. Weisbuch, Intrinsic mechanism for the poor luminescence properties of quantum-box systems, Phys. Rev. B **44**, 10945 (1991).

[44] H. T. Jiang and J. Singh, Radiative and non-radiative inter-subband transition in self assembled quantum dots, Physica E **2**, 720 (1998).